catalysts

MDPI

Article

Adsorption of VOCs Is a Key Step in Plasma-Catalyst Coupling: The Case of Acetone onto TiO_2 vs. CeO_2

Xianjie Wang [1], Christelle Barakat [1], Zixian Jia [1], Manolis N. Romanias [2], Frédéric Thévenet [2,*] and Antoine Rousseau [1,*]

[1] Laboratoire de Physique des Plasmas, Ecole Polytechnique, Sorbonne Université, Centre National de la Recherche Scientifique, CEDEX, 91128 Palaiseau, France; xianjie.wang@lpp.polytechnique.fr (X.W.); christelle.barakat@lpp.polytechnique.fr (C.B.); zixian.jia@gmail.com (Z.J.)

[2] Institut Mines Télécom Lille Douai, SAGE, Université de Lille, 59000 Lille, France; emmanouil.romanias@imt-lille-douai.fr

* Correspondence: frederic.thevenet@imt-lille-douai.fr (F.T.); antoine.rousseau@lpp.polytechnique.fr (A.R.)

Abstract: If a number of literature studies point at the positive role of coupling materials with non-thermal plasma, particularly for Volatile Organic Compounds (VOC) removal, most of them focus on the direct plasma-material interaction to understand the coupling. However, a key contribution relies in the VOC–material interaction. Therefore, this study focuses on the adsorption step of targeted VOCs to provide a new insight on plasma–material coupling. The adsorption of acetone, used as probe VOC, is explored on two widespread coupling materials: TiO_2 and CeO_2. First, their behaviors are compared regarding acetone uptake. This process is reactive and creates other organic species than acetone on both surfaces. Second, the metal oxide behaviors are compared regarding ozone uptake. Interestingly, under typical VOC treatment configuration, i.e., with organics on their surfaces, ozone uptake is driven by the adsorbed organics, not directly by the metal oxides anymore. Finally, the ozonation of both materials, preliminary exposed to acetone, is explored through the evolution of the adsorbed organics and the corresponding mineralization, i.e., CO and CO_2 formation. It evidences that the reactive adsorption of VOCs plays a key role in making the surface organics ready for an efficient oxidation and mineralization under post-plasma exposure.

Keywords: adsorbed phase; TiO_2; CeO_2; VOC oxidation; ozonation; non thermal plasma; plasma-catalysis

check for updates

Citation: Wang, X.; Barakat, C.; Jia, Z.; Romanias, M.N.; Thévenet, F.; Rousseau, A. Adsorption of VOCs Is a Key Step in Plasma-Catalyst Coupling: The Case of Acetone onto TiO_2 vs. CeO_2. *Catalysts* **2021**, *11*, 350. https://doi.org/10.3390/catal11030350

Academic Editors: Jean-François Lamonier and Annemie Bogaerts

Received: 2 February 2021
Accepted: 1 March 2021
Published: 9 March 2021

Publisher's Note: MDPI stays neutral with regard to jurisdictional claims in published maps and institutional affiliations.

Copyright: © 2021 by the authors. Licensee MDPI, Basel, Switzerland. This article is an open access article distributed under the terms and conditions of the Creative Commons Attribution (CC BY) license (https://creativecommons.org/licenses/by/4.0/).

1. Introduction

When the synergetic effect resulting from the coupling of non-thermal plasma with materials was evidenced in the early 2000s, the origin of such a positive interaction for the removal of pollutants was questioned and addressed. If the coupling materials can positively affect the discharge physics [1], the observed synergy was rapidly evidenced to be chiefly contributed by the material properties. First, the specific surface provided by the solid to the gas phase and to the plasma generated species was identified as a driver of the coupling process [2]. This point promoted the coupling of non-thermal plasma discharges with solids characterized by high porosity and large specific surface area such as zeolites and activated carbons. Further, the composition and the surface chemistry of the coupling material was evidenced as the key driver of the coupling, for the in-plasma and for the post-plasma configuration [3,4]. These findings oriented the investigation of the plasma-catalyst coupling toward the exploration of the surface processes involved [5] and the development of relevant experimental approaches to explore the underlying heterogeneous physical chemistry [6,7].

In the perspective of using plasma catalysis for Volatile Organic Compounds (VOC) removal [8], it is considered that the most interesting materials are generally able to (i) use oxidative plasma species to maintain their surface oxidation state and (ii) provide

sorptive and reactive surface sites to the processed VOCs and their organic byproducts. For these reasons, silica and alumina were progressively discarded, other metal oxides such as TiO_2 and CeO_2 were preferred since the 2010s. Based on the rich literature dealing with VOC removal by plasma, catalysis and their combinations, review papers such as the work of Chung et al. [9] proposed systematic analyses of the available data. If their approach allows drawing general trends between the different reactor configurations and catalysts deployed, the detailed comparisons of the performances of coupling materials using a reference experimental protocol is scarcely proposed. For instance, TiO_2 and CeO_2 are considered as well-known metal oxides respectively in the field of photocatalysis and thermal catalysis. Nonetheless, no accurate comparison of their behaviors based on the same pollutants, protocols and experimental conditions has been proposed yet. Beyond the comparison of their performances, assessing properly their individual actions can provide an informative contrast to enlarge our knowledge on the interactions between non-thermal plasma and metal oxide surfaces, especially when the treatment of organics is envisaged.

In the case of the post-situ configuration of plasma-catalysis for VOC treatment, the experimental sequence typically consists in adsorbing first the targeted compound on the coupling material. The importance of the adsorption step of organics on the coupling material is generally undermined, while it is a key step of the processing of organic pollutants by the plasma catalytic system. In a second step, the material covered by VOCs, up to a certain surface coverage, is exposed to the outlet gas flow of the plasma reactor. Adsorbed VOCs are subsequently exposed to long lifetime plasma species, i.e., ozone as a major oxidant. It should be mentioned that a number of VOCs could undergo reactive adsorption on metal oxides during the uptake step. This point has been clearly stated by Arsac et al. [10], Batault et al. [11], Thevenet et al. [12] and Barakat et al. [13]. It means that the performance of the plasma–catalytic system cannot be solely predicted from the reactivity of ozone with the primary VOC to be treated, since a variety of VOC byproducts, resulting from condensation or dissociation surface processes, can be present on the material as the plasma is ignited. Similarly, depending on the surface coverage of the coupling material by VOCs, ozone sent on the material surface does not necessarily interact with the coupling material, but rather with adsorbed organics. It suggests that the performance of the treatment is not only controlled by ozone decomposition on the material, but also by the reaction rates of oxidants with the different organics adsorbed on the material surface. In that context, Wang et al. [14] and Sultana et al. [15] proposed advanced investigation of the surface reaction pathways underlying the processing of methanol and trichloroethylene respectively. Beyond process investigations, these works emphasize the relevance of concomitantly investigating the fate of VOCs and oxidants in both the gas phase and adsorbed phase.

This work combines the investigation of the gas phase and the adsorbed phase. The post-plasma configuration is selected because it allows the in-situ monitoring of the surfaces of TiO_2 and CeO_2 by infrared (IR) spectroscopy while the materials, preliminarily covered by organics, are exposed to the discharge outlet gas flow. The selection of acetone as a model and probe VOC is motivated by (i) its representativeness in the domain of air quality and air treatment [16] and (ii) its foremost occurrence as VOC oxidation product [10,17,18]. Acetone also offers a definite number of byproducts, making the diagnosis and exploration of its reaction pathway in plasma–catalytic systems more accessible [13].

The objectives of this work are twofold. First, it aims at providing a comparative investigation of the individual behaviors of TiO_2 and CeO_2 combined with non-thermal plasma under the same experimental conditions. Second, this study aims at highlighting some less explored steps of the plasma–catalytic process, especially the adsorption step of primary VOCs and the evolution of the complex organic phase onto the surface of the coupling material under ozonation. This work aims at deepening our understanding of the contribution of the surface properties of coupling materials in the plasma–catalytic systems applied to VOC removal. It is structured as follows:

(i) The sorptive properties of metal oxides are examined qualitatively and quantitatively.

(ii) The individual abilities of TiO_2 and CeO_2 to decompose ozone generated by the upstream plasma is evaluated under different surface states, i.e., fresh and covered by acetone.

(iii) The evolution of the surface oxidation product is addressed to highlight and compare the surface reactivity of metal oxides induced by the upstream plasma reactor in the presence of adsorbed organics.

2. Results

2.1. Acetone Uptake on TiO_2 and CeO_2

Adsorbed phase monitoring: In order to evaluate the individual uptakes of acetone on TiO_2 and CeO_2, the materials were successively exposed to 200 ppm of acetone inside the diffuse reflectance infrared Fourier transform device (DRIFT) cell (setup (b) on Figure 1). Figure 2a,c respectively reports the DRIFT spectra of TiO_2 and CeO_2 surfaces upon acetone uptake at 294 K using 20% O_2 in Ar as bath gas. Spectra are recorded in the range 3200–1000 cm^{-1} with subtraction of the unexposed fresh material spectra as backgrounds.

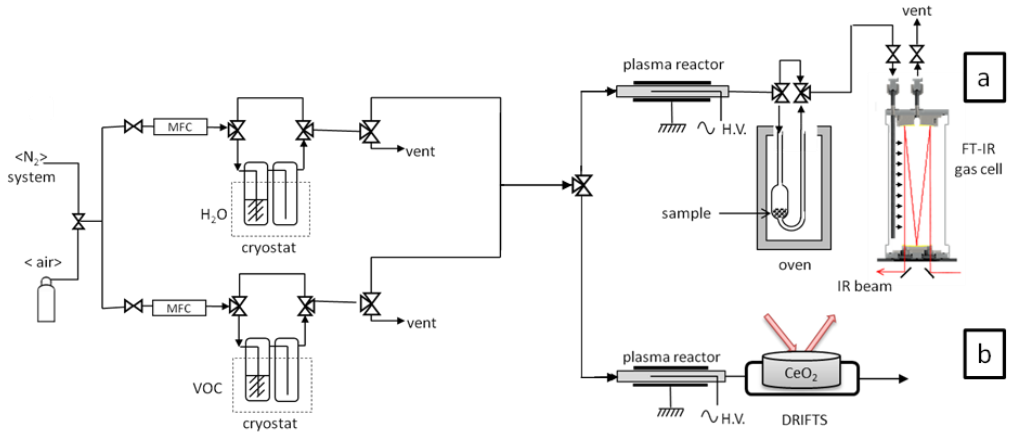

Figure 1. Schematic representation of experimental setups equipped with (**a**) gas phase FTIR monitoring device and (**b**) surface analysis by diffuse reflectance infrared Fourier transform device (DRIFT).

The presence of surface species on both metal oxides once acetone is introduced in the DRIFT cell is attested by the growth of various absorption bands with time on their respective DRIFT spectra. Noticeably the DRIFT spectra of acetone uptake on CeO_2 and TiO_2 exhibited similarities and contrasts. In order to interpret these infrared absorption patterns, literature data were collected to assign the bands observed to the corresponding groups.

Acetone uptake on TiO_2: Typical absorption bands were observed at 2972, 2937, 2921, 2869, 1705, 1697, 1667, 1595, 1469, 1450, 1422, 1380, 1365 and 1236 cm^{-1} (Figure 2a). The νC=O stretching vibration at 1705 and 1697 cm^{-1}, the δCH_3 at 1422–1365 cm^{-1} and the δC-C bending at 1236 cm^{-1} attest of the presence of adsorbed acetone species [19]. The temporal evolution of acetone adsorbed on TiO_2 surface is reported in Figure 2b from the integration of its characteristic band of absorption at 2972 cm^{-1}. As the uptake of acetone was initiated, the intensity of the characteristic bands sharply increased during the first 10 min of exposure. It suggest that the adsorption equilibrium of acetone was reached rapidly; nonetheless, a gradual decrease in the surface coverage of acetone was noticed beyond 10 min of exposure while the inlet concentration of acetone was kept constant. This behavior suggests possible consumption of acetone on the surface of TiO_2 once a significant surface coverage is reached.

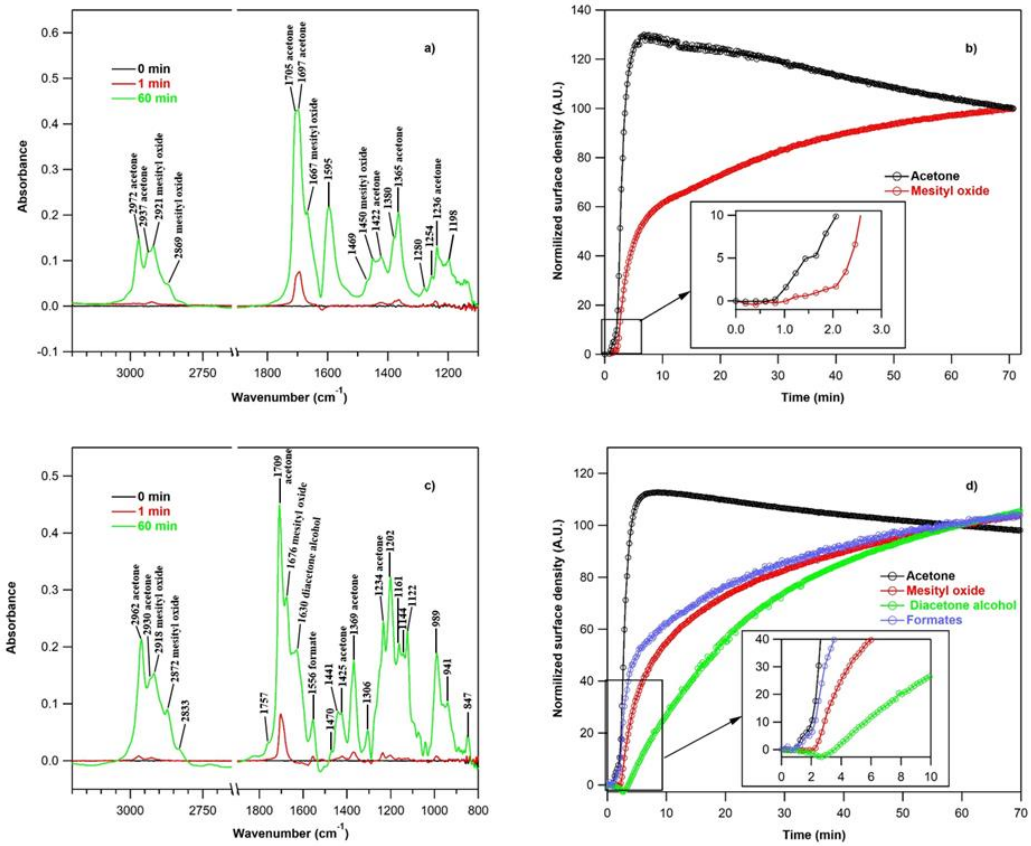

Figure 2. DRIFT monitoring of acetone uptake and TiO_2 and CeO_2 (200 ppm acetone, 250 mL/min 20% O_2 in Ar, 294 K): (**a**) DRIFT absorbance spectra recorded during acetone uptake on TiO_2. (**b**) Temporal profiles of acetone and mesityl oxide (MO) adsorbed on the surface of TiO_2 during the uptake of acetone. (**c**) DRIFT absorbance spectra recorded during acetone uptake on CeO_2. (**d**) Temporal profiles of adsorbed acetone, MO, formates and diacetone alcohol (DAA) on the surface of CeO_2 during the uptake of acetone.

Conversion of adsorbed acetone on TiO_2: Indeed, other surface absorption bands continuously increase on the DRIFT spectra in Figure 2a. Interestingly, these bands located at 1667, 1595 and 1450 cm^{-1} can be assigned to the typical vibration modes of mesityl oxide (MO) [20]. The temporal evolution of MO surface coverage is displayed along with acetone in Figure 2b. It is retrieved after integration of the absorption band at 1450 cm^{-1}. The observation of MO on TiO_2 surface has formerly been attributed to surface condensation and dehydration reactions of acetone molecules by Coronado et al. [21], El-Maazawi et al. [17], Xu et al. [16] and Barakat et al. [13]. The temporal evolution of MO on the TiO_2 surface is reported in Figure 2b. Between acetone and MO temporal profiles, a noticeable delay is visible on Figure 2b. Barakat et al. [13] and El-Maazawi et al. [17] interpret delay as a surface coverage threshold in acetone to initiate the formation of MO. Our observations confirm the existence of a threshold to induce acetone condensation and dehydration. Assuming that saturation of the surface is reached when acetone reaches its maximum at t = 8 min, we estimate the surface coverage threshold at 0.2, in accordance with former values reported at ca. 0.3. It has to be noted that diacetone alcohol (DAA) was identified and reported as a reaction intermediate of acetone condensation to form MO, but it was not observed on the DRIFT spectra recorded along acetone uptake on TiO_2. This suggests that the conversion rate of DAA into MO on TiO_2 was high enough not to allow any accumulation on the surface.

Acetone uptake on CeO_2: The introduction of acetone in the DRIFT cell containing CeO_2 initially resulted in the formation of specific bands at 2962, 2930, 1695, 1425, 1369 and 1234 cm^{-1} (Figure 2c). These bands were respectively assigned to νs-CH_3, ν_{as}-CH_3, $\nu C{=}O$, δ_{as}-CH_3, δ_s-CH_3 and νC-C vibration modes of adsorbed acetone. In the course of adsorp-

tion, at approximately 5 min, the band at 1695 cm^{-1} started splitting into two bands, at 1709 and 1676 cm^{-1}, along with new increasing bands at 1630, 1577, 1556, 1441, 1202, 1122 and 989 cm^{-1} (Figure 2c), attesting of other adsorbed species than acetone [22].

Conversion of adsorbed acetone on CeO_2: The band at 1630 was assigned to νC=O and δCH vibrations in -CH_2-C=O groups of diacetone alcohol-like species (DAA) [20]. Furthermore, the band at 1676 cm^{-1} was characteristic of the νC=O and νC=C vibration modes of MO. A very broad band, appearing in the range 3500–3600 cm^{-1} (not displayed in Figure 2c), accompanied them. It is assigned to dissociatively adsorbed H_2O, resulting from the dehydration of DAA molecule upon its conversion into MO. The peak at 1556 cm^{-1} also attested a contribution from the νOCO vibration of the formate species, which could be expected on the CeO_2 surface.

The adsorption of acetone on CeO_2 led to molecularly adsorbed acetone. It is gradually transformed into three condensation products: DAA, MO and formates. Their time evolution is reported in Figure 2d by monitoring the normalized peak areas of the different species: νC=O of DAA at 1630 cm^{-1}, νC=C of MO at 1676 cm^{-1} and ν_{as}COO of formates at 1556 cm^{-1}.

According to the evolution of products adsorbed on CeO_2 surface reported in Figure 2d, in the first five minutes, no condensation products were yet observed. During this time lapse, acetone gradually accumulated on CeO_2 surface until a maximum. Then it gradually decreased concomitantly with the formation of MO, DAA and formates. The increase in MO was faster than that of DAA, the intermediate between acetone condensation and MO. This could be consistent with a fast initial consumption of the intermediate, hindering its accumulation on the surface. Indeed, DAA was highly reactive and rapidly dehydrated to MO. As the surface became gradually covered, the formation of DAA was slowed down as the likelihood of condensation of two acetone molecules diminishes. Formates also gradually accumulated on the CeO_2 surface. In accordance with former observations reported for IPA adsorption on CeO_2, acetone was converted into carboxylate species, formates ($HCOO^-$), via a mechanism certainly involving lattice oxygen [20]. This type of reactive adsorption is observed on transition metal oxides, with readily accessible multiple oxidation states [23,24]. On these oxide surfaces, the condensation of acetone into MO is reported to start beyond a surface coverage of 0.28 as for TiO_2. Profiles reported in Figure 2d supported the existence of a coverage threshold regarding acetone conversion to MO.

Reactive adsorption pathway of acetone: Based on the work of Zaki et al. [20] the following steps of acetone reactive adsorption on CeO_2 were proposed. In most of the metal oxides, Mn^+ sites typically act as Lewis acids and the O_2^- ions act as Lewis bases. First, acetone initially adsorbs on the surface of Lewis acid sites (Ce^{4+}). If no basic site is available in the vicinity, acetone remains adsorbed on the metal center. If basic sites (-OH^- or O_2^-) are available, the C-H bond may be activated for α-hydrogen abstraction and the consequent formation of an anionic enolate-type ion. This allows the reaction of the enolate species with another acetone molecule, if the surface coverage of acetone is high enough, to lead to a DAA intermediate. Finally, dehydration of DAA leads to adsorbed MO and $H_2O_{(g)}$ or $H_2O_{(ads)}$. MO can be considered as the final product of acetone reactive uptake on CeO_2 and on TiO_2. If intermediate species, namely formates and DAA are observed on CeO_2, this is not the case on TiO_2. Assuming that similar reaction steps occur on both metal oxides, intermediates are likely to be formed on the TiO_2 surface as well, but directly consumed, suggesting of a higher surface reaction kinetic on TiO_2 for that step. According to the proposed mechanism, Lewis acid sites are essential for anchoring acetone molecules to the surface. Coexisting base sites catalyze the condensation of the acetone molecules into mesityl oxide surface species, via formation and subsequent decomposition of enolate and diacetone alcohol species.

The Lewis acid and base sites generate pairs of particularly efficient adsorption capacity toward condensation products thus formed. Consequently, before any plasma

exposure of the metal oxides with adsorbed acetone, surface reactions are already initiated, changing the nature of the organics in the adsorbed phase on CeO_2 and TiO_2.

Gas phase analysis: a quantitative approach of acetone uptakes: To improve the characterization of acetone adsorption on the TiO_2 and CeO_2 surface, adsorbed amounts of acetone are determined using experimental set up (a) allowing the breakthrough curve methodology as reported by Jia et al. [6]. Figure 3 reports the respective values of specific surface areas of both oxides and the irreversibly adsorbed amounts of acetone expressed in µmol/g respectively for TiO_2 and CeO_2. The specific surface of TiO_2 (45 ± 5 m^2/g) was lower than the one of CeO_2 (75 ± 5 m^2/g). However, the adsorption capacity of TiO_2 and CeO_2 should be considered from a surface density of acetone taken up, expressed in µmol/m^2. The surface density of acetone molecules adsorbed on TiO_2 was 2.64 µmol/m^2 and that of CeO_2 was 2.13 µmol/m^2. This result shows that both metal oxides provide a surface density of sorption sites for acetone in the same order of magnitude. The experimental value determined for TiO_2 exceeded that of CeO_2 by 20%, which might promote condensation reactions between acetone molecule and could possibly be consistent with a higher kinetic in MO formation on TiO_2.

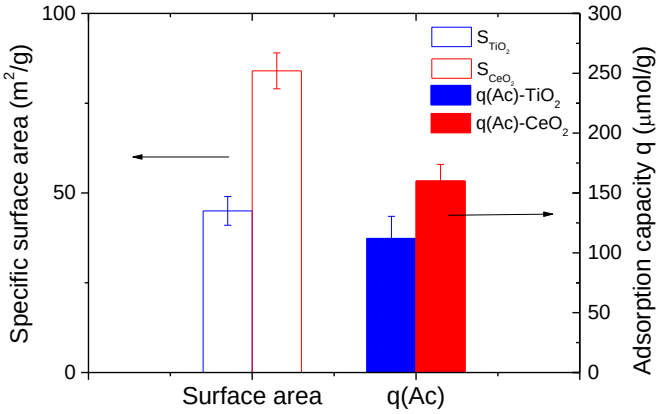

Figure 3. Features of TiO_2 and CeO_2 surfaces. On the left, specific surface areas of TiO_2 (S_{TiO2}) and CeO_2 (S_{CeO2}) expressed in m^2/g. On the right, quantity of irreversibly adsorbed acetone (q) expressed in µmol/g on TiO_2 (q(Ac)-TiO_2) and CeO_2 (q(Ac)-CeO_2).

2.2. Interaction of OZONE with TiO_2 and CeO_2: Impact of Adsorbed Acetone

The aim of the present section was to understand the similarities and differences of the interaction of ozone produced by plasma with CeO_2 or TiO_2 under different surface states, i.e., clean surface vs. covered by acetone. This approach addressed qualitatively and quantitatively the reactive behavior of ozone on both oxides. The breakthrough curves of ozone were monitored using the set up (a) (U-shape reactor and FT-IR) dedicated to gas phase monitoring and described in Figure 1. Once set in the U-shape reactor, both materials were treated first under dry air at 400 °C. Then two different cases were compared. First, exposure of the clean CeO_2 or TiO_2 to a 22 or 24 ppm ozone flow of 750 mL/min in order to monitor the uptake of ozone. Second, the materials were preliminarily exposed to 200 ppm of acetone for 60 min, as described in Section 2.1, then flushed using dry air, and subsequently exposed to a 22 or 24 ppm and 750 mL/min ozone flow. In the second case, the ozone interacts with a surface equilibrated with acetone. Note that the exact ozone concentration was respectively 22 ppm and 24 ppm for TiO_2 and CeO_2.

Since, it is not experimentally achievable to have simultaneously the same BET surface for both metal oxides, the same masses of materials and the same absolute amount of acetone taken up on each material, the following compromise was defined. The mass of material and BET surface were 200 mg, i.e., 9 m^2 for TiO_2, and 100 mg, i.e., 7.5 m^2 for CeO_2. Hence, the amount of acetone irreversibly adsorbed before ozone exposure was 23 µmol on TiO_2 and 16.5 µmol on CeO_2. Therefore, we reached a surface density of 2.6 µmol/m^2 for TiO_2 and 2.2 µmol/m^2 for CeO_2, consistently with the previous section. Figures 4 and 5

respectively reported the temporal profiles of the ozone concentration at the outlet of reactor, and the corresponding concentration of the ozone consumed.

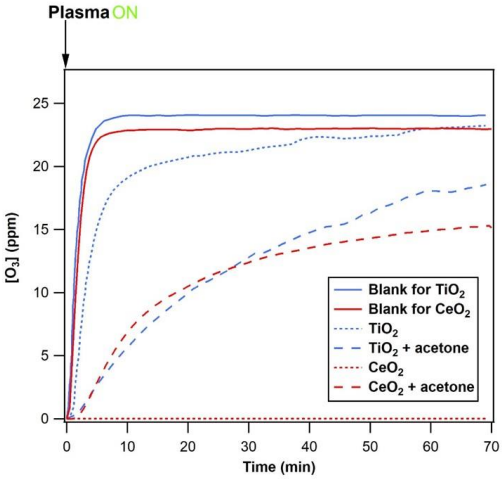

Figure 4. Temporal evolution of ozone concentration at the U-shape reactor outlet under 5 different conditions. (i) Without material in the U-shape reactor, i.e., ozone mixing curve. (ii) With 100 mg fresh CeO_2. (iii) With 100 mg CeO_2 covered by 2.2 µmol/m^2 of acetone. (iv) With 200 mg fresh TiO_2. (v) With 200 mg TiO_2 covered by 2.6 µmol/m^2 acetone. Flow rate = 750 mL/min, During the ozonation induced by non-thermal plasma $[O_3]_0$ = 22 ppm for CeO_2, $[O_3]_0$ = 24 ppm for TiO_2 and acetone is preadsorbed according to the protocol described in the previous adsorption section.

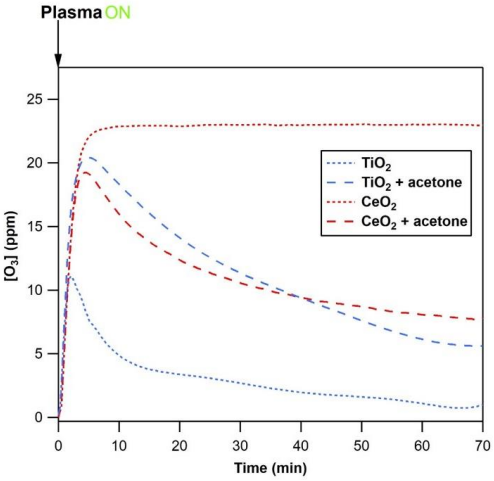

Figure 5. Temporal evolution of the difference between inlet and outlet ozone concentrations in the U-shape reactor under 5 different conditions: (i) Without material in the U-shape reactor, i.e., ozone mixing curve. (ii) With 100 mg fresh CeO_2. (iii) With 100 mg CeO_2 covered by 2.2 µmol/m^2 of acetone. (iv) With 200 mg fresh TiO_2. (v) With 200 mg TiO_2 covered by 2.6 µmol/m^2 acetone. Flow rate = 750 mL/min, During the ozonation induced by non-thermal plasma $[O_3]_0$ = 22 ppm for CeO_2, $[O_3]_0$ = 24 ppm for TiO_2, acetone is preadsorbed according to the protocol described in the previous adsorption section.

Without preadsorbed acetone, the clean ceria is a highly effective ozone decomposer compared to clean TiO_2. In the case of ceria, during 60 min of 22 ppm O_3 exposure, no ozone was detected downstream the U-shape reactor. At the opposite, ozone breaks through TiO_2 beyond 40 min of exposure only. TiO_2 transiently induced the decomposition of a fraction of ozone through its molecular and dissociative adsorption on Lewis acid sites (Ti^{3+} and Ti^{4+}). Ti is a Group IV transition metal and Ce is a lanthanide. Beyond the electronic structure, the polarity, the coordination of the cation, the surface lattice and the

corresponding surface vacancies are drivers of the surface properties of the solids. For metal oxides, the polarity of the surface and the degree of coordinative saturation of the metal cations are known as the driving forces of adsorption. The presence of a dipole moment increases the surface Gibbs energy, making a polar surface more unstable and more reactive than a non-polar one. However, more prominently, the coordinatively unsaturated surface atoms are central for adsorption and reactivity. With a lower number of nearest neighbors than their corresponding ions in the bulk, metal cations have underpopulated d orbitals and become active in bonding with adsorbates in order to increase their coordination number and lower their surface energy through chemisorption. In metal oxides, the coordination unsaturated M+ sites behave like Lewis acids and the O_2^- ions behave like Lewis bases. Acetone, and ketones in general, initially adsorb molecularly on metal oxides through a σ bond between the metal atom of the solid and the carbonyl oxygen atom of the molecule. The electron rich carbonyl oxygen donates an electron pair to the surface acting as a Lewis base, and the surface metal center acts as a Lewis acid by accepting the electron pair.

Bulanin et al. [25] showed that there are three main modes for ozone adsorption on TiO_2: (i) weakly bonded molecules that form hydrogen bonds with OH groups and are physically adsorbed on the surface; (ii) molecules adsorbed on the weaker Lewis acid sites and (iii) ozone interaction with strong Lewis acid sites. However, only ozone adsorbed on strong Lewis sites leads to the dissociation of the molecule. The continuous increase in concentration at the outlet of the sorbent reactor indicates that the decomposition efficiency of ozone decreases with time. This behavior is consistent with an increasing coverage of strong Lewis acid sites, making them gradually less available for further ozone adsorption. In 1998, Bulanin et al. [26] also reported the uptake of O_3 on CeO_2. Using electron-paramagnetic resonance, IR and kinetic studies, they show the formation of a surface ozonide species generated by the reaction of ozone with the electron rich surface sites on CeO_2. Alike TiO_2, they revealed two kinds of Lewis acid sites, where ozone can either adsorb. They also show that ozone can form weak hydrogen bonds with the most acidic OH groups on the surface. On acidic oxides such as alumina and titanium dioxide, O_3 activation and decomposition was shown to occur via dissociation on strong Lewis sites [23]. In the case of ceria, however, another non-dissociative mechanism of O_3 decomposition, involving unstable ozonide formation on surface basic oxygen sites was also observed. The enhanced dissociation in the case of CeO_2, as compared to TiO_2, could thus be attributed to this additional decomposition mechanism. However, does ozone chiefly interact with the material surface when organics are involved?

With preadsorbed acetone, the behavior of ozone is strongly altered on both oxides. On the one hand, the presence of acetone greatly inhibits the ozone uptake in the case of ceria. On the other hand, it is markedly enhanced in the case of TiO_2. The inhibition observed in the case of ceria may be due to the blockage of basic sites responsible for ozone dissociation by acetone decomposition products [24]. However, it is worth noticing that the ozone outlet concentration (Figure 4) and ozone consumption (Figure 5) are very similar for both materials covered by taking up acetone with equivalent surface densities of acetone. This result indicates that, the behavior of ozone on materials covered by organics did not mainly depend on the nature of the materials, but it was driven by the presence of the organics. It could also be noted that during the first minutes of exposure to ozone, if the uptake was close to 100%, it gradually decreased to 20% for precovered TiO_2 and 40% for precovered CeO_2.

The similar trends in ozone behavior observed for TiO_2 and CeO_2, preliminarily exposed to acetone indicate that, at high surface coverages, the adsorbed organics drive the uptake and reactivity of ozone, rather than the material itself. In order to get a better understanding of surface oxidation processes, CO and CO_2 production in the gas phase, and the evolution of adsorbed intermediates were investigated.

2.3. Ozonation of Acetone Adsorbed on TiO_2 and CeO_2

Monitoring of surface organics during ozonation of acetone exposed TiO_2 and CeO_2:

In the following, ozonation of TiO_2 and CeO_2, preliminarily exposed to 200 ppm acetone was monitored deploying the DRIFT technique (Figure 1, setup (b)). After the adsorption step, the reversible fraction of acetone was flushed under dry air during 60 min. As ozone was sent on the surface of TiO_2 or CeO_2, the reversible fraction with acetone adsorbed was removed by flushing and only the irreversible fraction of organics remained on the adsorbed phase of metal oxides. Note that the surface reaction involving adsorbed acetone molecules and leading to surface byproducts was still effective along the flushing step. The conversion of acetone taken up still contributed to the modification of the organic phase during that step. Figure 6a,c respectively reports DRIFT spectra collected during the ozonation of irreversibly adsorbed acetone on TiO_2 (a) and CeO_2 (c) surfaces in 20% O_2/80% Ar gas mixture at 294 K. DRIFT spectra are displayed in the range 3200–1000 cm^{-1} with subtraction of the spectra of the respective unexposed materials as backgrounds. Figure 6a,c evidenced that the oxidation of the surface organics by ozone occurred on TiO_2 and on CeO_2. If formates are observed in both cases, each material shows a different reactivity. A specific analysis of each case is described in the following.

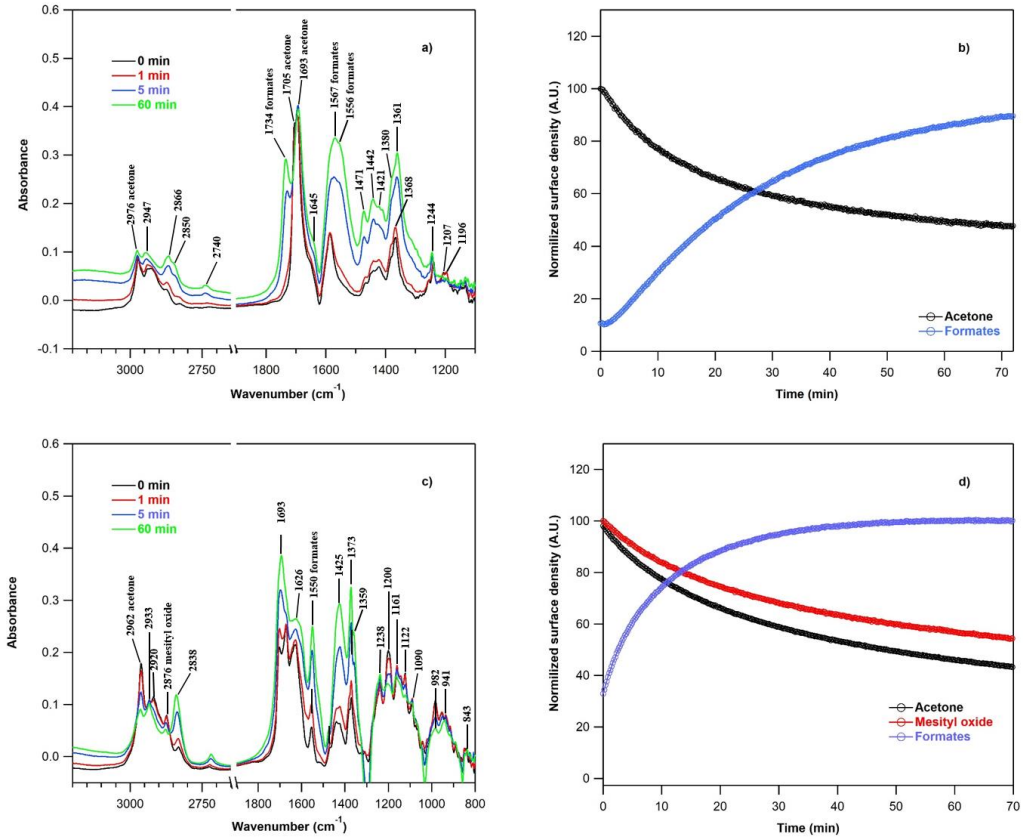

Figure 6. DRIFT monitoring of the ozonation of TiO_2 and CeO_2, preliminarily exposed to 200 ppm acetone, 250 mL/min 20% O_2 in Ar, 294 K, and flushed under dry air. (**a**) DRIFT absorbance spectra recorded during the ozonation of TiO_2 preliminarily exposed to acetone. (**b**) Temporal profiles of adsorbed acetone and formates on the surface of TiO_2 during the ozonation. (**c**) DRIFT absorbance spectra recorded during the ozonation of CeO_2 preliminarily exposed to acetone. (**d**) Temporal profiles of adsorbed acetone and intermediates (mesithyloxide (MO) and formate) on the surface of CeO_2 during the ozonation.

Ozonation of TiO_2 preliminarily exposed to acetone: DRIFT monitoring: As discussed in the previous section, acetone adsorption on TiO_2 results in molecularly adsorbed acetone and a main condensation product, MO. Exposing the saturated surface to ozone results in the oxidation of the organics at the expense of a new adsorbed product: formates. DRIFT spectra and temporal evolution of adsorbed organics are reported in Figure 6a,b respectively. Acetone was monitored through the evolution of the narrow band at 2976 cm^{-1} to avoid

peak overlapping with the products formed. As the discharge was turned on, the peak at 1667 cm^{-1}, corresponding to the νC=C of MO was broadened, probably because of formates gradually accumulating on the TiO_2 surface. The presence of surface formates was attested by the increasing band between 1567 and 1556 cm^{-1}. It is confirmed by a new peak at 1734 cm^{-1}, attributed to the νC=O vibration of carboxylic structure.

Ozonation of CeO_2 preliminarily exposed to acetone: DRIFT monitoring: DRIFT spectra and temporal profiles corresponding to the ozonation of CeO_2, preliminarily exposed to acetone, are reported on Figure 6c,d. At t = 0, the surface consisted of three other compounds than acetone: MO (νC=C = 1676 cm^{-1}), DAA (νC=O = 1630 cm^{-1}) and formate species ($\nu_{as}COO$) at 1556 cm^{-1} (Figure 2c). Exposing the surface to ozone resulted in a decrease in the intensities of the methyl stretching and bending frequencies of MO and DAA. The band 1693 cm^{-1} could be ascribed to formates, interacting with surface basic sites [27]. Meanwhile, the bands at 1556, 1373 and 1359 cm^{-1} could be assigned to the νCOO stretch of formate species upon acetone adsorption, and become more intense. Figure 6d shows that MO, a condensation product present on the surface after the adsorption and flushing steps, decreased at the expense of formates, gradually accumulating on the CeO_2 surface.Figure 5 shows that ozone decomposition on the surface in the first five minutes was concomitant with the significant MO loss and formate production Figure 6d. The surface coverage of formates remained relatively constant throughout the ozonation period. It suggests that the surface had reached a steady state, determined either by saturation of the adsorption sites and/or by the dynamic equilibrium between the carboxylates formation and consumption.

Mineralization and carbon balance during ozonation of acetone exposed TiO_2 and CeO_2.

The production of CO and CO_2 in the gas phase during the ozonation of acetone exposed TiO_2 and CeO_2 was investigated using the U shape reactor coupled to the 10 m optical-path white-cell (Figure 1, setup (a)). Figure 7 reports the temporal profiles of CO and CO_2 monitored in the gas phase during ozone exposure of TiO_2 and CeO_2 preliminarily exposed to 200 ppm acetone. Figure 8 reports the corresponding mineralization percentage defined as the ratio of the total number of moles of CO and CO_2 produced divided by the irreversibly adsorbed number of moles of acetone according to Equation (1). In that Equation, $X(t)$ represents the mineralization percentage as a function of time t, $(Ace)_0$ represents the number of mole of acetone irreversibly adsorbed before ozonation starts, [CO] and [CO_2] represent the concentration in ppm of CO and CO_2, and Φ is the total molar flow corresponding to 750 mL/min and equals to 5.13×10^{-4} mol/s.

$$X(t) = \frac{\Phi}{3(Ace)_0} \int_0^t [\mathrm{CO} + \mathrm{CO_2}]dx \quad (1)$$

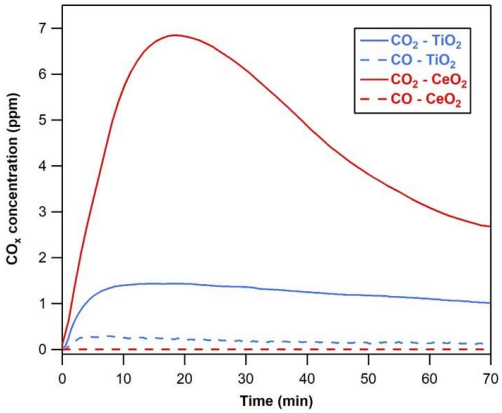

Figure 7. Temporal evolutions of CO and CO_2 at the U-shape reactor outlet during the ozonation of CeO_2 and TiO_2, preliminarily exposed to acetone (flow rate = 750 mL/min, $[O_3]_0$ = 22 ppm for CeO_2 experiments, $[O_3]_0$ = 24 ppm for TiO_2; 100 mg CeO_2, 200 mg TiO_2).

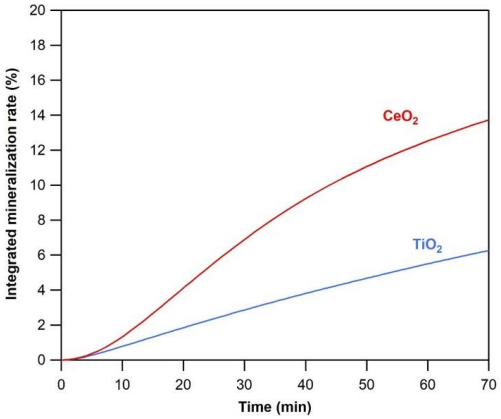

Figure 8. Temporal evolutions of the mineralization percentages of organics adsorbed on TiO_2 and CeO_2 along the individual exposure to ozone of the metal oxides preliminarily exposed to acetone; reported data are derived from Figure 7 (flow rate = 750 mL/min, $[O_3]_0$ = 22 ppm for CeO_2 experiments, $[O_3]_0$ = 24 ppm for TiO_2; 100 mg CeO_2, 200 mg TiO_2).

Comparing the temporal profile of CO_2 and CO monitored at the downstream of TiO_2 vs. CeO_2 reactors emphasizes contrasted mineralization regimes. First, for CeO_2, concentrations of CO remained below the detection limits of the instrument (i.e., 10 ppb) while in the case of TiO_2 from 0.2 to 0.4 ppm CO were produced on the whole investigated time span. CO_2 profiles confirmed contrasted behaviors. In the case of CeO_2, CO_2 production exhibited a characteristic transient regime while in the case of TiO_2, CO_2 production was lower (ca. 1 ppm) but remained rather constant on the experimental time.

The contrasted CO_2 dynamics may sound unexpected since: (i) the absolute amounts of acetone taken up on TiO_2 (23 µmol) exceeded the one taken up on CeO_2 (16 µmol); while (ii) the amounts of O_3 consumed were equivalent between both systems. One hypothesis to explain these contrasted behaviors relies on the fact that the oxidation pathway differs between TiO_2 and CeO_2, not directly because of their different chemical natures, but because they induce differences in the chemical nature of the adsorbed organics. More precisely, the high and transient formation of CO_2 using CeO_2 (Figure 7) suggests that, as the ozonation is initiated, a significant fraction of the organic phase adsorbed on CeO_2 is more compliant with the ozone reaction than organics adsorbed on TiO_2. In spite of the fact that TiO_2 and CeO_2 have preliminarily adsorbed the same initial VOC, namely acetone, they induce a significant conversion of acetone on their surface into surface intermediates. This reactive adsorption is effective on both oxides, with similar pathways, but with contrasted kinetics, leading to the presence of similar (mesithyl oxide) and different (DAA and formate) oxidation intermediates.

Consequently, the higher mineralization percentage observed in Figure 8 for CeO_2 was not due to a higher consumption of ozone or a higher amount of organics present on its surface, but rather to a difference in the nature of organic adsorbates compared to TiO_2. From that point of view, the mineralization ability of a metal oxide under post-plasma exposure is driven by its ability to induce reactive adsorption of the primary VOC and conversion to organics readily mineralized.

3. Discussion

Differences and similarities between CeO_2 and TiO_2 towards the ozonation of adsorbed acetone can be pointed out. First, as mentioned in Section 2.1, although DRIFT spectra evidence that a fraction of adsorbed acetone was converted into MO. This fraction was completed, in the case of CeO_2, by the presence of adsorbed DAA and formates. Therefore, when the ozonation process started, CeO_2 was covered by a larger diversity of organics, than TiO_2. When material preliminarily exposed to acetone, i.e., covered by organics, were exposed to ozone, ozone consumption profiles on TiO_2 and CeO_2 surfaces became very similar (Figure 5). The modification of ozone consumption by adsorbed

organics, and the convergent behaviors of both materials evidence that ozone did not directly interact with metal oxides, but rather with organic species adsorbed, at least at high surface coverages. In that case the performance of the plasma-catalytic system could be driven by the reaction between plasma oxidants and adsorbed organics. Therefore, the reactivity of adsorbed species toward the ozone must be examined.

The reaction of ozone with acetone, DAA and formates is expected to be very slow and is unlikely to occur. On the contrary, MO is suggested to be the key compound initiating the oxidation chemistry on the surface of the materials. Indeed, it is clearly stated in the literature that ozone is a reactive electrophilic molecule attacking the double bond of unsaturated organic compounds through the known "criegee" mechanism. The subsequent cleavage of this ozonide leads to the formation of carbonyl compounds and excited biradical species that finally lead to the production of free °OH radicals with high yields. Therefore, we suggest that the ozone readily attacks the double bond of adsorbed MO through a Langmuir–Hinshelwood mechanism, forming the highly reactive °OH radicals. MO being present in the adsorbed phase of both metal oxide after acetone adsorption, this suggestion is consistent with the fact that oxidation was observed with both oxides as the ozonation starts. Once °OH radicals are formed, they lead the oxidation mechanism of other organics. Considering the gas-phase °OH rate coefficients of MO (k (298) = 1.03×10^{-10} cm^3 $molecule^{-1}$ s^{-1}) [28], DAA (k (298) = 5.27×10^{-12} cm^3 $molecule^{-1}$ s^{-1}) [29] and acetone (k (298) = 1.8×10^{-13} cm^3 $molecule^{-1}$ s^{-1}) [26], °OH radicals attack first MO and DAA, rather than acetone. Therefore, the reduced concentration levels of acetone noted in Figure 6b,d should not only be interpreted as a direct reaction of acetone with OH, but also as the conversion of acetone to balance the consumed DAA and MO since these last two were effectively oxidized. The formates noticed to be produced from the very beginning of ozone introduction could be formed either from the ozonolysis of MO or from the non-selective oxidation of organic species by °OH radicals.

This interpretation is supported by the temporal profile of CO_2 (Figure 7) showing that, for CeO_2, CO_2 increased rapidly during the first 15 min before decaying. However, at t = 15 min, only 3% of the initial adsorbed carbon was mineralized. The decay of the CO_2 production in the gas phase cannot be explained by a decrease of the total surface coverage. It is more likely related to the decrease of DAA and MO fraction on the surface, which have been mineralized first, leading to a hindering of the process. In the case of TiO_2, the CO_2 temporal profile shows a fast increase up to 1.4 ppm and then remained nearly stable with a concentration of 1 ppm after 70 min, which was consistent with a lower fraction of adsorbed MO and the absence of DAA.

Comparing the behaviors of widespread metal oxides coupled to post plasma does not only consist in exploring their respective abilities to interact with oxidative plasma species. Indeed, the investigation of the adsorption phase of the targeted organics provides key information on the nature of the organics adsorbed, as non-thermal plasma is ignited and how readily the adsorbed organics can be oxidized. Finally, the surface properties of metal oxides are essential to understand the plasma material coupling. However, this study evidenced that a key contribution of the coupling material is to convert primary VOCs into byproducts readily mineralized by plasma oxidants.

4. Materials and Methods

Chemicals and materials: The VOC used in this study was supplied by Sigma Aldrich (St. Louis, MO, USA) and provided in the liquid form with the following reference: Acetone, 270725, CHROMASOLV®, for HPLC, ≥99.9%. Air Liquide (Paris, France) supplies certified gas cylinders of air, nitrogen, oxygen and argon. CeO_2 powder supplied by Sigma Aldrich offers a specific surface of 75 ± 5 m^2/g. The TiO_2 powder was the P25 type from Degussa, its specific surface area was 45 ± 5 m^2/g. The specific surface areas of both materials were determined using a laboratory sorption analyzer using N_2 as probe gas.

Gas flow preparation: The regulation of the gas flows was insured using Brooks (Hatfield, PA, USA) mass flow controllers up to 2000 mL/min (±1%, i.e., less accurate

below an imposed flow of 20 mL/min). The mass flow controller used for VOC dilution had a maximum of 10 mL/min and was accurately used down to 0.1 mL/min. Experiments were typically performed using an acetone concentration of 200 ± 5 ppm. The gas inlet system was mutualized for the two complementary reactors: U-shape reactor coupled to FTIR in setup (a) and DRIFT cell in setup (b). (Figure 1). The U-shape reactor and DRIFT cell cannot be used in parallel. A two-way valve allows the selection of either air or N_2 as the main carrier gas. The flow was then divided into two lines, one of which could pass through the cryostat containing water (main flow) and the other through the cryostat containing the liquid VOC. For experiments under humid conditions, the main flow was sent through the water condensation/saturation system to be saturated with the targeted H_2O level. For dry conditions, the cryostat containing water was bypassed. The second line was used: (i) for calibration experiments or (ii) for diluting the VOC. The flow could be sent to vent or to the reactor when needed. If sample heating is required, the furnace can be moved to the reactor of setup (a).

Plasma reactors: One plasma reactor was set upstream from the U-shape reactor (setup(a)) and another one was set upstream from the DRIFT cell (setup (b)). Each setup constituted a post-plasma system. Each plasma reactor consisted of a Pyrex glass tube of 23.5 cm length, 3.3 mm external diameter and 1.7 mm inner diameter. The high voltage electrode was a tungsten wire of 0.2 mm thickness placed in the middle of the tube. The ground electrode consisted of a copper sheet wrapped around the dielectric Pyrex tube. The electrical parameters of reactors were measured via two high voltage probesLeCroy (Chestnut Ridge, New York, NY, USA) PPE20KV-CC connected to a digital oscilloscope (LeCroy WaveSurfer 64Xs-A, 600 MHz). A measurement capacitor (Cm) of 680 pF was placed in series with the dielectric barrier discharge (DBD) reactors. The injected power was obtained from the Lissajous figures, corresponding to the plotting of the transported electric charges through the discharge as a function of the periodical applied voltage.

Infrared diagnostics for GAS PHASE analysis: SETUP (a): For the real time detection and quantification of the gas phase species, the U-shape reactor of setup (a) was coupled to a high resolution Nicolet (Waltham, MA, USA) 6700 Fourier Transform Infrared spectrometer (FTIR) equipped with a 10 m optical-path white-cell and a cooled MCT (mercury cadmium telluride) detector (Figure 1, setup (a)). Two spectra per minute were collected with Omnic software with 16 scans per spectrum and a spectral resolution of 0.5 cm^{-1}. Detection limits of this analytical tool were determined as two times the signal/noise ratio in the region of interest and are: 80 ppb for acetone, 20 ppb for CO_2, 10 ppb for CO and 15 ppb for O_3.

Infrared diagnostics for ADSORBED PHASE analysis: SETUP (b): In the adsorbed phase investigation setup, materials were inserted inside the cell of the diffuse reflectance infrared Fourier transform device (DRIFT), placed downstream the plasma reactor as shown in Figure 1. In the DRIFT cell, the infrared beam was focused on the material surface. The sample holder was a ceramic crucible where materials were set. The cell contains a heating resistor to possibly heated the sample up to 800 °C. The temperature was directly monitored by a thermocouple in contact with the powder. Two spectra per minute were collected with Omnic software with 16 scans per spectrum and a spectral resolution of 4 cm^{-1}.

Author Contributions: X.W., C.B. and Z.J.: experiments, data treatment and formal analysis; M.N.R., F.T. and A.R.: data treatment and formal analysis, conceptualization, methodology, validation, writing, review and editing, project administration and funding acquisition. All authors have read and agreed to the published version of the manuscript.

Funding: This research was funded by Direction Generale de l'Armement (DGA), Labex Plas@Par and AL-KO SA. Authors acknowledge Ecole Polytechnique and CNRS; IMT Lille Douai participates in the Labex CaPPA project, funded by the ANR through the PIA under contract ANR-11-LABX-0005-01, and in the CLIMIBIO project, funded by the "Hauts-de-France" Regional Council and the European Regional Development Fund (ERDF).

Data Availability Statement: The data presented in this study are available on request from the corresponding author.

Acknowledgments: M.N.R., F.T. and A.R. are grateful to Mediterranean sea, for its warm light and rocky islands, Crete and Levant, to enjoy and face the rest of the year.

Conflicts of Interest: The authors declare no conflict of interest. The funders had no role in the design of the study; in the collection, analyses, or interpretation of data; in the writing of the manuscript, or in the decision to publish the results.

References

1. Ogata, A.; Yamanouchi, K.; Mizuno, K.; Kushiyama, S.; Yamamoto, T. Oxidation of Dilute Benzenein an Alumina Hybrid Plasma Reactor at Atmospheric Pressure. *Plasma Chem. Plasma Process* **1999**, *19*, 383–394. [CrossRef]
2. Holzer, F.; Roland, U.; Kopincke, F. Combination of non-thermal plasma and heterogeneous catalysis for oxidation of volatile organic compounds: Part 1. Accessibility of the intra-particle. *Appl. Catal. B* **2002**, *38*, 163–171. [CrossRef]
3. Chen, H.L.; Lee, H.M.; Chen, S.H.; Chang, M.B.; Yu, S.J.; Li, S.N. Removal of Volatile Organic Compounds by Single-Stage and Two-Stage Plasma Catalysis Systems: A Review of the Performance Enhancement Mechanisms, Current Status, and Suitable Applications. *Environ. Sci. Technol.* **2009**, *43*, 2216–2227. [CrossRef]
4. Sivachandiran, L.; Thevenet, F.; Rousseau, A. Isopropanol removal using Mn_XO_Y packed bed non-thermal plasma reactor: Comparison between continuous treatment and sequential sorption/regeneration. *Chem. Eng. J.* **2015**, *270*, 327–335. [CrossRef]
5. Bogaerts, A.; Tu, X.; Whitehead, J.C.; Centi, G.; Lefferts, L.; Guaitella, Q.; Azzolina-Jury, F.; Kim, H.H.; Murphy, A.B.; Schneider, W.F.; et al. The 2020 Plasma Catalysis Roadmap. *J. Phys. D Appl. Phys.* **2020**, *53*, 443001. [CrossRef]
6. Jia, Z.; Wang, X.; Thevenet, F.; Rousseau, A. Dynamic probing of plasma-catalytic surface processes: Oxidation of toluene on CeO_2. *Plasma Process. Polym.* **2017**, *14*, 1600114. [CrossRef]
7. Jia, Z.; Rousseau, A. Sorbent track: Quantitative monitoring of adsorbed VOCs under in-situ plasma exposure. *Sci. Rep.* **2016**, *6*, 31888. [CrossRef]
8. Thevenet, F.; Sivachandiran, L.; Guaitella, O.; Barakat, C.; Rousseau, A. Plasma-catalyst coupling for volatile organic compound removal and indoor air treatment: A review. *J. Phys. D Appl. Phys.* **2014**, *47*, 224011. [CrossRef]
9. Chung, W.C.; Mei, D.H.; Tu, X.; Chang, M.B. Removal of VOCs from gas streams via plasma and catalysis. *Catal. Rev.* **2019**, *61*, 270–331. [CrossRef]
10. Arsac, F.; Bianchi, D.; Chovelon, J.M.; Ferronato, C.; Herrmann, J.M. Experimental Microkinetic Approach of the Photocatalytic Oxidation of Isopropyl Alcohol on TiO_2. Part 1. Surface Elementary Steps Involving Gaseous and Adsorbed C_3H_xO Species. *J. Phys. Chem. A* **2006**, *110*, 4202–4212. [CrossRef]
11. Batault, F.; Thevenet, F.; Hequet, V.; Rillard, C.; Le Coq, L.; Locoge, N. Acetaldehyde and acetic acid adsorption on TiO_2 under dry and humid conditions. *Chem. Eng. J.* **2015**, *264*, 197–206. [CrossRef]
12. Thevenet, F.; Olivier, L.; Batault, F.; Sivachandiran, L.; Locoge, N. Acetaldehyde adsorption on TiO_2: Influence of NO_2 preliminary adsorption. *Chem. Eng. J.* **2015**, *281*, 126–133. [CrossRef]
13. Barakat, C.; Gravejat, P.; Guaitella, O.; Thevenet, F.; Rousseau, A. Oxidation of isopropanol and acetone adsorbed on TiO_2 under plasma generated ozone flow: Gas phase and adsorbed species monitoring. *Appl. Cat. B. Environ.* **2014**, *147*, 302–313. [CrossRef]
14. Wang, X.; Wu, J.; Wang, J.; Xiao, H.; Chen, B.; Peng, R.; Fu, M.; Chen, L.; Ye, D.; Wen, W. Methanol plasma-catalytic oxidation over CeO_2 catalysts: Effect of ceria morphology and reaction mechanism. *Chem. Eng. J.* **2019**, *369*, 233–244. [CrossRef]
15. Sultana, S.; Vandenbroucke, A.M.; Mora, M.; Jiménez-Sanchidrián, C.; Romero-Salguero, F.J.; Leys, C.; De Geyter, N.; Morent, R. Post plasma-catalysis for trichloroethylene decomposition over CeO_2 catalyst: Synergistic effect and stability test. *Appl. Cat. B Environ.* **2019**, *253*, 49–59. [CrossRef]
16. Kirchner, S.; Arenes, J.F.; Cochet, C.; Derbez, M.; Duboudin, C.; Elias, P.; Gregoire, A.; Jedor, B.; Lucas, J.P.; Pasquier, N.; et al. Etat de la qualite de l'air dans les logement francais. *Environ. Risques St.* **2007**, *6*, 250–269.
17. Larson, S.A.; Widegren, J.A.; Falconer, J.L. Transient Studies of 2-Propanol Photocatalytic Oxidation on Titania. *J. Catal.* **1995**, *157*, 611–625. [CrossRef]
18. Xu, W.; Raftery, D.; Fransisco, J.S. Effect of Irradiation Sources and Oxygen Concentration on the Photocatalytic Oxidation of 2-Propanol and Acetone Studied by in Situ FTIR. *J. Phys. Chem. B* **2003**, *107*, 4537–4544. [CrossRef]
19. El-Maazawi, M.; Finken, A.N.; Nair, A.B.; Grassian, V.H. Adsorption and Photocatalytic Oxidation of Acetone on TiO_2: An in Situ Transmission FT-IR Study. *J. Catal.* **2000**, *191*, 138–146. [CrossRef]
20. Rossi, P.F.; Busca, G.; Lorenzelli, V.; Saur, O.; Lavalley, J.C. Microcalorimetric and FT-IR spectroscopic study of the adsorption of isopropyl alcohol and hexafluoroisopropyl alcohol on titanium dioxide. *Langmuir* **1987**, *3*, 52–58. [CrossRef]
21. Coronado, J.M.; Kataoka, S.; Tejedor-Tejedor, I.; Anderson, M.A. Dynamic phenomena during the photocatalytic oxidation of ethanol and acetone over nanocrystalline TiO_2: Simultaneous FTIR analysis of gas and surface species. *J. Catal.* **2003**, *219*, 219–230. [CrossRef]
22. Zaki, M.I.; Hasan, M.A.; Pasupulety, L. Surface Reactions of Acetone on Al_2O_3, TiO_2, ZrO_2, and CeO_2: IR Spectroscopic Assessment of Impacts of the Surface Acid−Base Properties. *Langmuir* **2001**, *17*, 768–774. [CrossRef]

23. Sinha, A.K.; Suzuki, K.; Takahara, M.; Azuma, H.; Nonaka, T.; Fukumoto, K. Mesostructured manganese oxide/gold nanoparticle composites for extensive air purification. *Angew. Chem. Int. Ed. Engl.* **2007**, *46*, 2891–2894. [CrossRef]
24. Kung, H.H. *Transition Metal Oxides: Surface Chemistry and Catalysis*; Elsevier: New York, NY, USA, 1989.
25. Bulanin, K.M.; Lavalley, J.C.; Tsyganenko, A.A. Infrared Study of Ozone Adsorption on TiO_2 (Anatase). *J. Phys. Chem.* **1995**, *99*, 10294–10298. [CrossRef]
26. Bulanin, K.M.; Lavalley, J.C.; Lamotte, J.; Mariey, L.; Tsyganenko, N.M.; Tsyganenko, A.A. Infrared Study of Ozone Adsorption on CeO_2. *J. Phys. Chem. B* **1998**, *102*, 6809–6816. [CrossRef]
27. Zaki, M.I.; Hussein, M.; Mansour, S.; El-Ammawy, H. Adsorption and surface reactions of pyridine on pure and doped ceria catalysts as studied by infrared spectroscopy. *J. Mol. Catal.* **1989**, *51*, 209–220. [CrossRef]
28. Gaona-Colmán, E.; Blanco, M.B.; Teruel, M.A. Kinetics and product identification of the reactions of (E)-2-hexenyl acetate and 4-methyl-3-penten-2-one with OH radicals and Cl atoms at 298 K and atmospheric pressure. *Atmos. Environ.* **2017**, *161*, 155–166. [CrossRef]
29. Aslan, L.; Laversin, H.; Coddeville, P.; Fittschen, C.; Roth, E.; Tomas, A.; Chakir, A. Kinetics of the photolysis and OH reaction of 4-hydroxy-4-methyl-2-pentanone: Atmospheric implications. *Atmos. Environ.* **2017**, *150*, 256–263. [CrossRef]